

THE MOTT TRANSITION AND f ELECTRON PHYSICS

GABRIEL KOTLIAR

*Serin Physics Laboratory, Rutgers University,
Piscataway, New Jersey 08855-0849*

SERGEJ Y. SAVRASOV

*Department of Physics, New Jersey Institute of Technology,
Newark, New Jersey 07102*

Received 13 July 2001

We revisit the issue of the Mott transition across the actinide series from the perspective of the spectral density functional approach to realistic dynamical mean-field theory. We stress both qualitative insights from the connection with models and quantitative results.

1. Introduction

The Mott transition, namely the metal-insulator transition (MIT) driven by electron-electron interactions, is a fascinating phenomenon realised experimentally in many compounds such as V_2O_3 and $Ni(Se,S)_2$. It was suggested many years ago by Johansson that the Mott transition concept is also relevant to elements in the lanthanide and actinide series.¹ The development of dynamical mean-field methods, and the solution of the Mott-transition problem within this methodology, has spurred the development of new electronic structure methods, and qualitative and quantitative insights into the physics of actinides. Johansson's observation placing Pu near a localisation-delocalisation boundary is a key to understanding this complex material and other localisation-delocalisation transitions such as the α to γ transition in elemental Cerium. The appropriate technique for developing this idea is the dynamical mean-field method.²

Non self-consistent studies of alpha gamma Cerium have appeared in Ref. 3. In Section 2 we discuss some qualitative aspects of the physics which are less dependent on microscopic detail, and that can be understood by allowing volume fluctuations in the model Hamiltonian phase diagram. Quantitative work on Pu⁴ using a framework described in Section 3 will be discussed in Section 4, in relation to other methods.

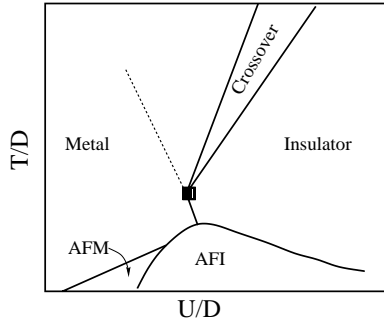


Fig. 1. A schematic phase diagram of partially frustrated Hubbard model from Ref. 6

2. 4f and 5f Electron Systems: Qualitative Discussion

The development of the dynamical mean-field theory (DMFT) has clarified a great deal the workings of the localisation delocalisation transition or crossover. It was shown formally, in Ref. 5, that the low energy description of the Mott transition within DMFT is a Kondo model satisfying a self consistency condition.

There are two phase diagrams which summarise the results of many investigations.² The first one one exactly at integer filling, is described in Fig. 1. The finite temperature transition between the localised and extended regime as a function of the ratio of the interaction U to the bandwidth, takes place via a first order transition.² At high temperatures the phase diagram of Ref. 6 displays two

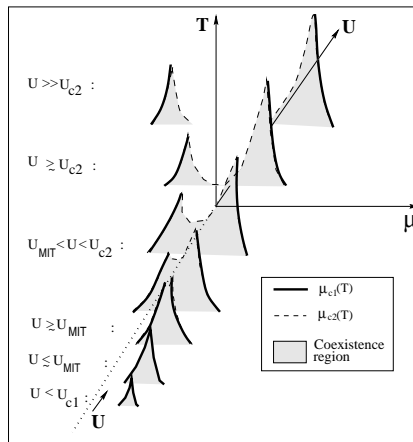


Fig. 2. Schematic phase diagram for the degenerate Hubbard model. The cross sections shown are on the T - μ plane for different values of U . μ_{c1} (the heavy line) U_{c1} are the chemical potential and interaction respectively at which the insulating solution gets destroyed. μ_{c2} (the dotted line) and U_{c2} are the chemical potential and interaction at which the metallic solution gets destroyed. U_{MIT} is the value of the interaction at which the MIT takes place. The shaded regions are where the metallic and the insulating solutions coexist.

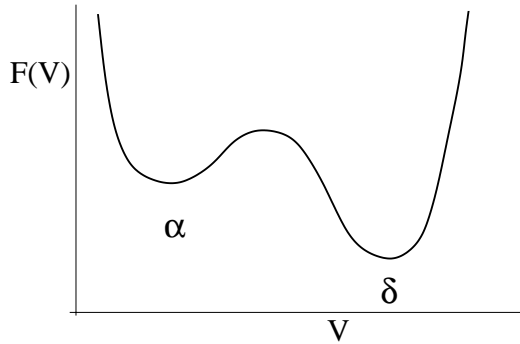


Fig. 3. Schematic drawing of the free energy vs volume, obtained by allowing the volume to fluctuate in a system near the Mott transition. The larger volume has lower energy and could be identified with the delta phase of Pu, while the smaller volume has higher free energy and represents a caricature of the alpha phase

crossover lines. The dotted line in Fig. 2 is a coherence incoherence crossover (i.e. the continuation of a U_{c2} line where metallicity is lost). The second crossover region (explicitly indicated as a crossover in Fig. 2) is a continuation of a U_{c1} line, where the insulating behaviour disappears because the temperature becomes comparable with the gap.

Introducing a finite chemical potential to allow for density changes leads to the schematic phase diagram described in Fig. 2.⁷ It is a natural extension of the previous phase diagram, indicating various regions of phase coexistence. At a generic doping driven finite temperature Mott endpoint the compressibility diverges.⁷

To understand the structure of materials, one needs to include the effect, allowing the relaxation of other degrees of freedom, in addition to the ones included in the simple Hubbard model.^{4,8} These degrees of freedom include the various deformations of the unit cell necessary to reach the different crystal structures and the actual volume of these materials, as well as additional bands.

We now present a simple qualitative argument connecting the model Hamiltonian phase diagrams 1 and 2 and a striking feature of Smith-Kmetko phase diagram.⁹ The minimum and the melting temperature correlates with the location of the Mott transition point which occurs near the Mott transition between Neptunium and Plutonium. According to the Clausius–Clayperon equation, at the melting curve:

$$dT/dp = \frac{V_s - V_l}{S_s - S_l} \quad (1)$$

A minimum in the melting curve requires that $V_s - V_l$ changes sign as pressure is varied. The stable phase at low pressure resembles the more localised-like solution whose volume is larger than that of the liquid phase, to allow for spin-orbital entropy gain, while at high pressure the state is described by the more itinerant solution which has a volume smaller than that of the liquid to gain kinetic energy (this is

done via an increase of the hybridisation term in a realistic multiband description). The essential point is that the volume of the liquid phase varies slowly with pressure, while the volume of the solid phase varies very rapidly near the Mott transition endpoint where the compressibility diverges. As a result the position of the zero in Eq. (1), when the system passes near the Mott transition endpoint.

Notice that a similar minimum occurs near the critical pressure necessary to transform alpha to gamma Cerium, supporting an universal mechanism related to the closeness of a finite temperature Mott endpoint.¹⁰

Allowing the coupling of volume fluctuations to the Mott transition point, results in a double-minimum structure in the energy vs. volume curve.^{4,8} The larger volume minima corresponds to the solution which is more localised, while the smaller volume minima can be continued from the more itinerant state in the coexistence region of the phase diagram in Fig. 1. This situation may explain the unusual negative thermal expansion observed in delta Pu if the activation energy to the more itinerant metastable minima is small enough to overcome the usual positive thermal expansion arising from thermal fluctuations inside a single minima in which case the total volume described by

$$V(T) = V_\delta(T) + V_\alpha(T)e^{-E/T} \quad (2)$$

can decrease as temperature increases.

3. Functional Formulation and Hybrid Schemes

There are many problems where only some degrees of freedom are strongly interacting, requiring sophisticated and (computationally costly) many-body techniques while other degrees of freedom cannot be ignored but can be handled by simpler methods such as density functional theory (DFT).

The basic idea to merge DFT and DMFT is to introduce two relevant variables: the density and the local Green function. The latter is defined by projecting the full Green function onto a separate subset of correlated orbitals distinguished by the index a from a complete set of orbitals $\chi_a(\mathbf{r} - \mathbf{R}) \equiv \chi_{\alpha R}$ (labeled by α) of a tight-binding representation which we assume for simplicity to be orthogonal. It is therefore given by a matrix \hat{G} with elements¹¹

$$G_{ab}(i\omega) = -\langle c_a(i\omega)c_b^\dagger(i\omega) \rangle = -\int \chi_a^*(\mathbf{r})\langle \psi(\mathbf{r}, i\omega)\psi^\dagger(\mathbf{r}', i\omega) \rangle \chi_b(\mathbf{r}') d\mathbf{r}d\mathbf{r}'. \quad (3)$$

We then construct a functional $\Gamma[\rho, \hat{G}]$ of both ρ and the local Green function $\hat{G}(i\omega)$ which gives the exact free energy at stationary point. This generalises the effective action construction used in connection with either pure dynamical mean-field functionals¹¹ or pure density functionals.¹² It amounts to first considering the partition function of the interacting electron gas, in the presence of a static source coupled to the density and dynamic source coupled to the local spectral function, and, second, carrying out a Legendre transformation with respect to those sources. This functional can be constructed formally in perturbation theory, however its

explicit form is not available just as is the case in density functional theory. The success of DMFT in model Hamiltonians suggests a useful approximation to the exact functional, namely the LDA+DMFT functional which allows us to compute total energies in addition to providing a consistent derivation¹³ of the realistic LDA+DMFT equations which had been formulated earlier.¹⁴

In terms of the density the local Greens function, their conjugate fields and a local interaction matrix \hat{U} we write down the DMFT+LDA functional:

$$\begin{aligned} \Gamma_{LDA+DMFT}(\rho, V_{KS}, \hat{G}, \hat{\Sigma}) = & -T \sum_{i\omega} \text{tr} \log[i\omega + \nabla^2 - V_{KS} - \Sigma] - \int V_{KS}(\mathbf{r})\rho(\mathbf{r})d\mathbf{r} \\ & - \sum_{i\omega} \text{Tr} \hat{\Sigma}(i\omega) \hat{G}(i\omega) + \int V_{ext}(\mathbf{r})\rho(\mathbf{r})d\mathbf{r} \quad (4) \\ & + \frac{1}{2} \int \frac{\rho(\mathbf{r})\rho(\mathbf{r}')}{|\mathbf{r} - \mathbf{r}'|} d\mathbf{r}d\mathbf{r}' + E_{xc}^{LDA}[\rho] + \Phi[\hat{G}] - \Phi_{DC}. \end{aligned}$$

$\Phi[\hat{G}]$ is the sum of local diagrams constructed with the local interaction matrix \hat{U} , and the local heavy propagator \hat{G} , which are two particle irreducible. Φ_{DC} is the so called double counting term which subtracts the average energy of the heavy level already described by LDA. We write it here in its simple form, when only one Slater integral is included in the approach, i.e. $\Phi_{DC} = \bar{U}\bar{n}(\bar{n} - 1)/2$ with $\bar{n} = T \sum_{i\omega, ab} G_{ab}(i\omega) e^{i\omega 0^+}$ (see Ref. 15 for its general form). Other choices of the double counting correction have also been used in the context of the LDA+U method.

An explicit form of $\Phi[\hat{G}]$ is unavailable. Furthermore its perturbative expansion is very misleading a fact that was recognised very early on¹⁶ and lead to a reformulation in terms of atomic quantities and a Weiss field. This insight, leads us to relate $\Phi[\hat{G}]$ to the free energy of an atom in a medium, W_{at} . The atom described by an action S_{at} . To do it we introduce the second central concept of DMFT: the Weiss field G_0^{-1} representing the quadratic part of the action S_{at} :

$$\begin{aligned} S_{at}[G_0^{-1}] = & \int_{\tau\tau'} \sum_{ab} c_a^+(\tau) G_{0ab}^{-1}(\tau, \tau') c_b(\tau') \\ & + \int_{\tau} \sum_{abcd} U_{abcd} c_a^+(\tau) c_b^+(\tau) c_c(\tau) c_d(\tau). \quad (5) \end{aligned}$$

Here, $\hat{G}_0^{-1} = \hat{G}_{at}^{-1} - \hat{\Delta}$ where \hat{G}_{at}^{-1} describes the quadratic part of the action of the isolated atom, and $\hat{\Delta}$ describes the bath surrounding the atom. It is the bath that added to the atomic action produces the desired local Green function i.e. $\langle c_a c_b^+ \rangle_{S_{at}} = G_{ab}$. We can now relate the sum of local graphs $\Phi[\hat{G}]$ to the free energy of the atom in the medium $W_{at} = -\log \int \exp[-S_{at}]$ via

$$\Phi[\hat{G}] = W_{at}[\hat{G}_0^{-1}] - \text{Tr}(\hat{G}_0^{-1} - \hat{G}^{-1})\hat{G} - \text{Tr} \log \hat{G}. \quad (6)$$

The functional (5) can be viewed as a functional of four independent variables, since the stationary condition in the conjugate fields reproduces the definition of the dynamical Kohn–Sham field and the Weiss field. Extremising it leads us to compute the Green function $G_{ab}(i\omega)$, (3) with the Kohn–Sham potential entering $H_{\alpha\beta}^{\mathbf{k}}$ (this matrix is just an expression of the one particle Kohn–Sham Hamiltonian in a tight binding basis) and with

$$\Sigma_{ab}(i\omega) = \frac{\delta\Phi}{\delta G_{ab}(i\omega)} - \frac{\delta\Phi_{DC}}{\delta G_{ab}(i\omega)}, \quad (7)$$

which identifies $\Sigma(i\omega)$ as the self-energy of a generalised Anderson impurity model in a bath characterized by a matrix of levels

$$\epsilon_{ab} = \sum_{\mathbf{k}} H_{ab}^{\mathbf{k}} \quad (8)$$

hybridised with the medium via hybridisation function $\Delta_{ab}(i\omega_n)$. The matrix $\delta\Phi_{DC}/\delta G_{ab}(i\omega) = \bar{U}(\bar{n} - 1/2)$ takes into account the double counting effects of Coulomb interaction already contained in matrix $H_{ab}^{\mathbf{k}}$. The hybridisation function $\Delta_{ab}(i\omega)$ obeys the self-consistency condition

$$i\omega - \epsilon_{ab} - \Delta_{ab}(i\omega) = \Sigma_{ab}(i\omega) + \left[\sum_{\mathbf{k}} [i\omega - \hat{H}^{\mathbf{k}} - \hat{\Sigma}(i\omega)]^{-1} \right]_{ab}^{-1}. \quad (9)$$

The self-consistent loop with respect to $\hat{\Delta}(i\omega)$ and $\hat{\Sigma}(i\omega)$ is known as DMFT loop which amounts to: (i) fixing some input hybridisation $\hat{\Delta}(i\omega)$, (ii) solving the Anderson impurity model and extracting the impurity Green function and self-energy $\hat{\Sigma}(i\omega)$, and (iii) recovering a new hybridisation function $\hat{\Delta}(i\omega)$ from the Eq. (9) after performing the \mathbf{k} integration. Since the charge density depends on $\hat{\Sigma}(i\omega)$, another self-consistent loop is required to obtain the extremum of Eq. (5). It updates the charge density once the DMFT loop delivers the self-energy, which modifies the one-electron Hamiltonian (hopping integrals). The new hoppings set up a new set of impurity levels and we see that the solution of Eqs. (7)–(9) should be carried out in a double iterative loop: the DMFT loop one finds $\hat{\Sigma}(i\omega)$ for given ρ while the global one (DFT like) updates ρ . This framework was fully implemented recently, and resulted in quantitative insights into the delta phase of Plutonium.⁴

4. Delta Plutonium: DMFT View and Comparison with other Methods

δ *Pu* is an anomalous metal. To begin density functional calculations grossly underestimate its volume by up to 35%.^{17–19} If the *f* electron is included as core, then density functional grossly overestimate the volume. This is very anomalous since even in strongly correlated materials such as the high-temperature superconductors, LDA predicts volume with 5% accuracy and even phonons with good accuracy.

A second puzzle has to do with the nature of the α phase. This phase's volume is correctly predicted by LDA. The transport and thermodynamic properties of α and δ are very similar, and have received so far no explanation. For a review see Ref. 20, more recent measurements are reported in Ref. 21.

Several approaches have been implemented to address these puzzles. The LDA+*U* method was applied to δ Pu in Refs. 18 and 19. It is able to produce the correct volume of the delta phase, for values of the parameter *U* consistent with first principles calculations. The drawback of this method is that its inability to predict correct excitation spectrum. The group in Los Alamos, has proposed a constrained LDA approach in which 4 of the 5*f* electrons, are treated as core,

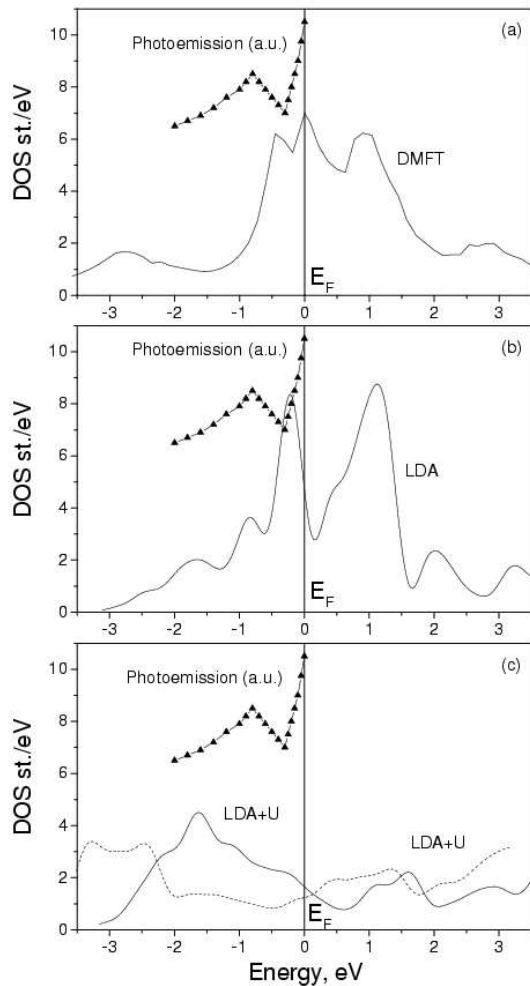


Fig. 4. Comparison between calculated density of states for δ -Pu using various methods (lines) and the photoemission experiments (symbols).²¹ (a) Dynamical mean-field calculation (b) Local density approximation, (c) LDA+*U* method with two possible choices of double-counting terms.

while the remaining one is allowed to participate in band formation.²² The dynamical mean-field theory has been fully implemented and applied to this problem in Ref. 4.

To compare the results of the dynamical mean-field calculations with the LDA and LDA+U methods as well as with the experiments, we discuss the results presented in Fig. 4. Figure 4(a) shows the calculated density of states for δ Pu in the vicinity of the Fermi level (solid line)⁴ in comparison with the photoemission data.²¹ Both the quasiparticle peak and the lower and upper Hubbard bands can be clearly distinguished in this plot. The corresponding comparison within the local density approximation is shown on Fig. 4(b). The LDA produces two peaks near the Fermi level corresponding to $5f^{5/2}$ and $5f^{7/2}$ states separated by the spin-orbit coupling. The Fermi level falls into dip between these states and cannot reproduce the features seen in photoemission. Moreover the value of the density of states is too small to account for the measured specific heat. Figure 4(c) shows the comparison between our calculated density of states using the LDA+U method¹⁸ (solid and dashed lines) and the photoemission data (symbols). Two curves (solid and dashed) for the LDA+U calculations correspond to different double counting terms of the LDA+U method. We see that LDA+U fails completely to reproduce the intensity of the f -states near the Fermi level as it pushes the f -band 2-3 eV below the Fermi energy. This is the picture expected from the static Hartree–Fock theory as the LDA+U. Only full inclusion of the dynamic effects within the DMFT allows to account for both the quasiparticle resonance and the Hubbard satellites and explain all features of the photoemission spectrum in δ Pu.

Acknowledgments

This research was supported by the Division of Materials Research of the National Science Foundation, under grant NSF DMR 0096462, the Division of Basic Energy Sciences of the Department of Energy under grant US DOE, grant No. DE-FG02-99ER45761.

References

1. B. Johansen, *Phil. Mag.* **30**, 469 (1974); B. Johansen, *Phys. Rev.* **B11**, 2740 (1975).
2. For a review see A. Georges G. Kotliar W. Krauth and M. J. Rozenberg, *Rev. Mod. Phys.* **68**, 13 (1996).
3. J. Laegsgaard and A. Svane, *Phys. Rev.* **B58**, 12817 (1998); M. V Zofi *et al.*, cond-mat 0101280; K. Held *et al.*, cond-mat 0106599.
4. S. Savrasov G. Kotliar and E. Abrahams, *Nature* **410**, 793 (2001).
5. Moeller, G., Q. Si, G. Kotliar, M. J. Rozenberg and D. S. Fisher, *Phys. Rev. Lett.* **74**, 2082 (1995).
6. M. Rozenberg *et al.*, *Phys. Rev. Lett.* **75**, 105 (1995).
7. G. Kotliar S. Murthy and M. Rozenberg, in preparation.
8. Majumdar, P. and H. R. Krishnamurthy, *Phys. Rev. Lett.* **73**, 1525 (1994).
9. Smith J. L and E A Kmetko, *J. Less Common Metals* **90**, 83 (1983).

10. For a review see, *Handbook of the Physics and Chemistry of the Rare Earths*, Vol. 1, eds. K. A. Gschneider and L. Eyring North-Holland, Amsterdam, (1978).
11. R. Chitra and G. Kotliar, *Phys. Rev.* **B62**, 12715 (2000).
12. R. Fukuda, T. Kotani, and S. Yokojima, *Prog. Theor. Phys.* **92**, 833 (1994).
13. S. Savrasov and G. Kotliar, cond-mat 0106308.
14. V. Anisimov, A. Poteryaev, M. Korotin, A. Anokhin and G. Kotliar, *J. Phys. Cond. Mat.* **35**, 7359 (1997).
15. I. Y. Solovyev, A. Liechtenstein and K. Terakura, *Phys. Rev. Lett.* **80**, 5788 (1999).
16. A. Georges and G. Kotliar, *Phys. Rev.* **B45**, 6479 (1992).
17. P. Soderlind, O. Eriksson, B. Johansson and J. Wills, *Phys. Rev.* **B50**, 7291 (1994); M. D. Jones, J. C. Boettger, R. C. Albers and D. J. Singh, *Phys. Rev.* **B61**, 4644 (2000).
18. S. Y. Savrasov and G. Kotliar, *Phys. Rev. Lett.* **84**, 3670 (2000).
19. J. Bouchet, B. Siberchicot, F. Jollet and J. Pasturel, *Phys. Condens. Matter* **12**, 1723 (2000).
20. S. S. Hecker and Timofeeva, *Los Alamos Sci.* **26**, 244 (2000); A. J. Freeman and J. B. Darby (eds.) *The Actinides: Electronic Structure and Related Properties*, Vols. 1 and 2 (Academic, New York, 1974).
21. A. J. Arko, J. J. Joyce, L. Morales, J. Wills and J. Jashley, *Phys. Rev.* **B62**, 1773 (2000).
22. O. Eriksson, J. D. Becker, A. V. Balatsky and J. M. Wills, *J. Alloys Compd.* **287**, 1 (1999).